Image Segmentation Using Clique Based Shape Prior and the Mumford Shah Functional *

Frederick Park[†]

December 21, 2010

Abstract

A novel shape prior segmentation model is proposed that utilizes the cliques invariant signature along with a polygonal piecewise constant implementation of the Mumford-Shah Functional. The model will be shown to be useful in the context of difficult segmentation problems including and not limited to segmenting objects amongst clutter, or recognizing objects containing components with large scale non-uniform image intensities. In addition, the model will also be shown to be effective for image disocclusion. Lastly, the proposed model can accomplish all the aforementioned tasks both efficiently and with near automation.

Keywords: Shape prior segmentation, active contours, level set methods, disocclusion, total-variation, Chan-Vese model, Mumford-Shah model, shape averaging, invariant signature

1 Introduction

Shape prior segmentation is an elementary problem of image processing that takes in a priori information about a known shape to reduce ambiguity in image segmentation problems. It is a problem that has been around for quite some time and merges many concepts from cognitive psychology, computer science, engineering, and mathematics. In general, human cognition relies on previous experience to recognize objects; particularly amidst clutter or with occlusion. Shape prior segmentation attempts to tackle a similar problem where a particular shape signature is incorporated into existing segmentation models to aid in capturing appropriate boundaries of objects of interest.

From a a mathematical perspective, generally speaking, standard (non shape prior) image segmentation is a difficult problem. In a given image, there are many different possible segmentations occurring at differing scales. This particular trait also manifests itself into many existing segmentation models. For an explicit example, let us foremost consider the celebrated Mumford and Shah (MS) [32] segmentation model in 2-phase form:

$$E_{MS}(\Sigma, c_1, c_2) = \mathrm{Per}(\Sigma) + \lambda \int_{\Sigma} (c_1 - f)^2 \mathrm{dxdy} + \int_{\Sigma^c} (c_2 - f)^2 \mathrm{dxdy}. \tag{1}$$

Here, f is a given gray scale image (with regions to be segmented), Σ denotes a region, and Σ^c the outside of that region. The key idea is to minimize the above functional (1) by matching two regions (constants) in the L^2 sense while simultaneously minimizing the perimeter of the boundaries

*This work was partially supported by grants from the NSF under contract DMS-0713767.

†Department of Mathematics, University of California at Irvine, 340 Rowland Hall, Irvine, CA 92697-3875. Email: fepark@math.uci.edu

between them. The MS model is one of the most studied and successful segmentation models in image processing. However, one particular caveat of this model, given its variational nature, is that the functional has many local minimizers that can depend on the initial starting conditions (initial guess) that correspond to incorrect segmentations at differing scales. There have been many recent convexifications of the MS model, see [4, 13]. However, the non-uniquesness of minimizers often pose similar complications.

Given the already present challenges with image segmentation and the additional caveats of the MS model, certain settings can further compound these issues, if not outright making the problem nearly impossible to solve in a meaningful way (e.g. meaningful segmentations). Such cases include and are not limited to segmenting images amidst clutter (geometric noise), segmenting an object containing components with large scale non-homogenous image intensities, or segmenting objects near ones with similar intensities. For an explicit example of this, we can look to Fig. 1 where a segmentation of a plane is attempted by a polygonal version of the Mumford-Shah model. In Fig. 1 (a) an initial curve is observed while the resulting segmentation is seen in Fig. 1 (b) where the MS model is unable to correctly segment the airplane. The clutter and the fact that the plane contains components of differing intensities are the likely causes that exacerbate the problem, not to mention the contribution from the adjacent plane further complicating the segmentation. Therefore, in these settings (and possibly many others), unless some a priori information is incorporated into the standard segmentation model, tackling such problems are quite formidable at best.

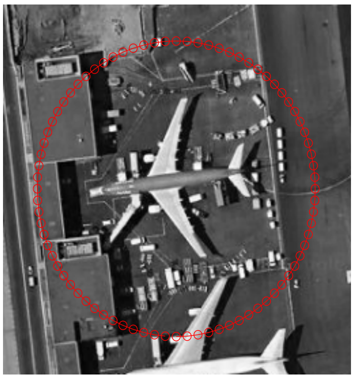

(a) Image and Initial Starting Curve

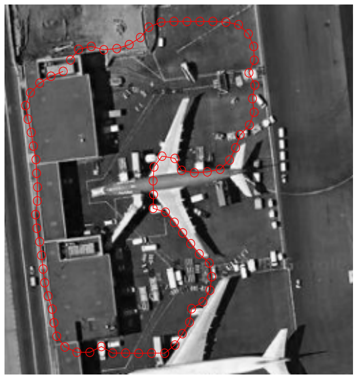

(b) Segmentation Result (No Shape)

Figure 1: *Segmentation Results, MS Functional:*

There are some key difficulties in building a successful shape prior segmentation model. Developing and/or utilizing a shape signature that is invariant under rigid motions while also simultaneously having the ability to uniquely identifying a broad class of shapes is paramount. Many useful signatures and references thereof can be found in [18, 9, 10] and we refer the reader there. Moreover, besides the beneficial invariance properties, the ability to incorporate such shape signatures naturally and efficiently into existing segmentation models is mandatory for applications. Developing a model under these two-fold conditions is quite difficult due to the limitations of both.

The key component of the approach in the paper is to incorporate a modified two dimensional version of the cliques signature proposed by Kimmel et al. [9, 10, 18] into a polygonal implementation of the two phase piecewise constant Mumford Shah model. Moreover, an efficient and nearly automated numerical algorithm for segmenting images in the difficult segmentation settings described earlier will be shown. Although many sophisticated numerical implementations of the

MS model exist utilizing level set methods, graph cuts, and more recently region based methods, the difficulty with these methods in the context of shape signatures is in incorporating such signatures based on those methods into the Mumford-Shah or other comparable segmentation models. Thus, the simplified version of the cliques energy utilized is conducive to the polygonal form of the Mumford-Shah functional that is fast, robust to noise, and easy to implement; all the while the utilized signature strongly identifies given shapes. Numerical examples will be shown to support these claims.

The contributions of this paper are summarized in bullet form below:

- Utilize the Cliques invariant signature with the Mumford-Shah Functional for shape prior image segmentation.
- Introduce a polygonal implementation of the Mumford-Shah functional.
- Introduce a fast, efficient, and nearly automated algorithm for minimizing the proposed energy in the context of difficult image segmentation and disocclusion problems.

Related work includes a level set based shape prior segmentation model proposed by Zhu and Chan in [46] that is motivated by the work by Cremers et. al [7] where the authors propose the use of a level set function for segmentation along with another labeling level set function to indicate the regions on which the prior shape should be compared. A fast method is also proposed and successful examples are shown of segmented objects amidst clutter (multiple objects). Another related model combining an active contour method, a geometric shape prior, and the Mumford-Shah functional is introduced by Bresson et al. in [5] for variational shape prior segmentation. The model is viewed as an extension of the one proposed by Chen et al. [14] where they incorporate the statistical shape model of Leventon et al. [26] along with the Mumford-Shah model [32]. Many successful numerical examples are shown and the method is a balance of region based and edge based approaches, however, registration of the prior is needed for the segmentations. The aforementioned models differ by the proposed one in the sense that the utilized signature with the proposed is completely invariant with respect to rigid motion and a polygonal version of the Mumford-Shah model is used allowing for fast segmentations with ease of implementation.

The paper is organized as follows: in section 2, we introduce our proposed model which includes the formal definition of the cliques invariant signature along with the polygonal piecewise constant implementation of the Mumford-Shah functional in two phase form. In section 3, we discuss the energy minimization associated to the proposed model, along with explicit numerical implementation and the final resulting algorithm. We demonstrate through comprehensive numerical experiments in section 4, the success of our model in the setting of arduous segmentation and disocclusion problems where the standard Mumford-Shah model has difficulties. Moreover, a method of averaging a set of shape priors in relation to the 'cliques' signature is also discussed. Lastly, in section 5, we give conclusions and future work, while in section 6 some acknowledgements.

2 Proposed Model

2.1 Invariant Signature: Cliques Energy

Let us foremost consider a polygonal representation of a given shape S: $S = \{\vec{r}_i\}_{i=1}^N$. Here, $\vec{r}_i = (x_i^r, y_i^r)$ the vertices of the polygon representing the given reference shape S. Now we consider d_{ij} which denotes the intervertex distances of a reference (i.e. library) shape that is:

$$d_{ij} = |\vec{r}_i - \vec{r}_j| \,. \tag{2}$$

Then, $[d_{ij}]$ is a symmetric matrix only depending on the given reference shape. The idea of cliques was proposed in the work by Elad and Kimmel [18] where the authors developed a bending invariant representation which is an embedding of the geometric structure of a given surface in a small dimensional Euclidean space in which geodesic distances are approximated by Euclidean ones. We consider the simplified version of the intervertex distances of uniformly distributed points on the boundary of a two dimensional shape. It is well known that above signature (2) has been shown to uniquely identify convex shapes and has been shown to be useful in its unabridged form for applications in surface classification [18] and face recognition [9, 10].

For the image segmentation, we consider an evolving polygon Σ: $\Sigma = \{\vec{p}_j\}_{j=1}^N$, where $\vec{p}_j = (x_j, y_j)$ denotes the vertices of said polygon with the same number of vertices of the reference shape S. Thus, our proposed shape signature utilizing the intervertex distances of a reference shape is given by:

$$\inf_{\Sigma,\, s} \left\{ E_C(\vec{p}_1, \vec{p}_2, \ldots, \vec{p}_N, s) = \sum_{i,j=1}^{N} \left(|\vec{p}_i - \vec{p}_j|^2 - s d_{ij}^2 \right)^2 \right\}. \tag{3}$$

The (symmetric) matrix $\{d_{ij}\}$ is to be computed only once, of course, at the beginning of the segmentation process, since it only depends on the given reference shape. The parameter: 's' is for scale invariance, and is to be minimized over as well. The shape signature (3) given above then has the following invariances:

- Invariance with respect to rigid motions, and
- Scale invariance.

For the remainder of the paper, we will call the shape signature energy (3), the 'Cliques' energy.

2.2 Proposed Shape Prior Segmentation Model

We propose to utilize the cliques invariant signature (3) with a polygonal implementation of the piecewise constant Mumford Shah Functional. Thus, our proposed shape prior segmentation model has the following formulation:

$$\begin{aligned} E(\Sigma, c_1, c_2, s) &= E_{MS} + E_C \\ &= \Big\{ \mathrm{Per}(\Sigma) + \lambda \int_{\Sigma} (c_1 - f)^2 \mathrm{dxdy} + \lambda \int_{\Sigma^c} (c_2 - f)^2 \mathrm{dxdy} \\ &\qquad + \alpha \sum_{i,j=1}^{N} \left(|\vec{p}_i - \vec{p}_j|^2 - s d_{ij}^2 \right)^2 \Big\} \\ &= E_{MSWS} \end{aligned} \tag{4}$$

Here, Σ is the evolving polygon, c_1 and c_2 are constants depending on average values of image intensities in the interior of Σ and Σ^c respectively, and 's' is a scale parameter depending on the recovered segmentation feature. As with our proposed shape signature (3), $\{\vec{p}_i\}$ are the vertices of the polygon Σ and $\{d_{ij}\}$ are the intervertex distances of a given reference shape. The parameter α dictates the strength of the shape prior. We also note that the acronym 'MSWS' stands for (Piecewise Constant) Mumford Shah With Shape. The main idea with the proposed model (4) is to determine, as seen in (1), the best approximation of a given image f in the L^2 averaged sense into two disconnected regions taking on only two values c_1 and c_2, while simultaneously enforcing that the given shape of the segmented region Σ be as close to a fixed reference shape as much as possible.

3 Energy Minimization and Numerical Implementation

3.1 Normal Speed of the Mumford-Shah Model

Although we will not use level sets for the numerical implementation of the proposed model (4), we will need the correct normal speed for the evolving curve in gradient descent in the implementation of it. Chan and Vese (CV) in their seminal work [15] proposed a level set formulation of the Piecewise Constant Mumford-Shah Model as follows:

$$E_{ACWE}(\phi, c_1, c_2) = \int_\Sigma |\nabla H_\epsilon(\phi)| \, + \, \lambda \int_\Sigma H_\epsilon(\phi)(c_1 - f)^2 \, + \, (1 - H_\epsilon(\phi))(c_2 - f)^2 \mathrm{dxdy}. \tag{5}$$

Here '$ACWE$' denotes Active Contours without Edges as proposed in [15]. The regions Σ and Σ^c are now represented by a regularized heaviside function H_ϵ of a level set function ϕ, where the zero level set $\{\phi = 0\}$ represents the boundary of Σ, and its interior is simply given by the upper level set $\{\phi > 0\}$.

The associated gradient descent flow to minimize the above CV model (5) is given by:

$$\phi_t \, = \, H'_\epsilon(\phi) \left\{ \nabla \cdot \frac{\nabla \phi}{|\nabla \phi|} \, + \, \lambda \left[(c_2 - f)^2 - (c_1 - f)^2 \right] \right\} \tag{6}$$

whose steady state solution coincides with the one associated to the morphological flow discussed in [44]:

$$\phi_t \, = \, |\nabla \phi| \left\{ \nabla \cdot \frac{\nabla \phi}{|\nabla \phi|} \, + \, \lambda \left[(c_2 - f)^2 - (c_1 - f)^2 \right] \right\}. \tag{7}$$

Thus, we can read off the correct normal speed of the curve in gradient descent from the above equation (7) as the following:

$$v \, = \, k \, + \, \lambda \left[(c_2 - f)^2 - (c_1 - f)^2 \right] \tag{8}$$

where k denotes the curvature of the evolving curve.

3.2 The Perimeter and Fidelity Terms of the Polygonal Mumford Shah Model

The minimization of the proposed model (4) is to be carried out over the set Σ and the two constants c_1 and c_2. In the polygonal curve based implementation, we restrict ourselves to the case where the set Σ is the interior of a polygon of N sides, whose vertices are given in counter-clockwise order as $(x_1, y_1), \ldots, (x_N, y_N)$. The perimeter term from the proposed model (4) is easy to represent in terms of the vertices:

$$\mathrm{Per}(\Sigma) \, = \, \sum_{j=1}^{N} \sqrt{(D^+ x_j)^2 + (D^+ y_j)^2} \tag{9}$$

with the proviso that $(x_{N+1}, y_{N+1}) \, = \, (x_N, y_N)$. Here, D^+ denotes the forward discrete difference operator:

$$D^+ \xi_j \, = \, \xi_{j+1} - \xi_j. \tag{10}$$

For the evolving polygon Σ, we have $(x_j, y_j) = (x_j(t), y_j(t))$. Now, differentiating the perimeter term in 't', we obtain:

$$
\begin{aligned}
\frac{d}{dt}\mathrm{Per}(\Sigma) &= \sum_{j=1}^{N} \frac{D^+x_j D^+\dot{x}_j + D^+y_j D^+\dot{y}_j}{\sqrt{(D^+x_j)^2 + (D^+y_j)^2}} \\
&= -\sum_{j=1}^{N} D^-\left(\frac{D^+x_j}{\sqrt{(D^+x_j)^2 + (D^+y_j)^2}}\right)\dot{x}_j + D^-\left(\frac{D^+y_j}{\sqrt{(D^+x_j)^2 + (D^+y_j)^2}}\right)\dot{y}_j \\
&= -\sum_{j=1}^{N} \vec{v}_j^1 \cdot (\dot{x}_j, \dot{y}_j)\sqrt{(D^+x_j)^2 + (D^+y_j)^2} \qquad (11)
\end{aligned}
$$

where we identify the vector $\vec{v}_j^1$ as:

$$
\vec{v}_j^1 = \frac{1}{\sqrt{(D^+x_j)^2 + (D^+y_j)^2}}\left(D^-\left(\frac{D^+x_j}{\sqrt{(D^+x_j)^2 + (D^+y_j)^2}}\right), D^-\left(\frac{D^+y_j}{\sqrt{(D^+x_j)^2 + (D^+y_j)^2}}\right)\right). \qquad (12)
$$

Now, the contribution of the fidelity term in the proposed model (4) to the normal speed of the polygonal curve will be:

$$
\vec{v}_j^2 = \lambda\left[(c_2 - f)^2 - (c_1 - f)^2\right]\vec{n}_j, \qquad (13)
$$

where $\vec{n}_j$ is the unit normal vector at the j-th vertex:

$$
\vec{n}_j = \frac{1}{\sqrt{(D^+x_j)^2 + (D^+y_j)^2}}\left(-D^+y_j, D^+x_j\right). \qquad (14)
$$

Finally, putting the contribution of the perimeter (12) and fidelity (13) terms together, and multiplying by a factor of $\sqrt{(D^+x_j)^2 + (D^+y_j)^2}$ (which improves stability and still leads to a descent direction), we get the the following ODE system describing the time evolution of vertices $(x_j(t),\, y_j(t))$ of the polygon:

$$
\begin{aligned}
\frac{d}{dt}(x_j(t),\, y_j(t)) &= \left(D^-\left(\frac{D^+x_j}{\sqrt{(D^+x_j)^2 + (D^+y_j)^2}}\right), D^-\left(\frac{D^+y_j}{\sqrt{(D^+x_j)^2 + (D^+y_j)^2}}\right)\right) \\
&+ \lambda\left[(c_2 - f)^2 - (c_1 - f)^2\right](-D^+y_j,\, D^+x_j) \qquad (15) \\
&= \vec{v}_j^{per} + \vec{v}_j^{fid}.
\end{aligned}
$$

Here, $\vec{v}_j^{per}$ and $\vec{v}_j^{fid}$ denote the velocities corresponding to the perimeter and fidelity terms for the polygonal piecewise constant implementation of the Mumford-Shah model respectively.

3.3 Update of the constants c_1 and c_2

In the original piecewise constant Mumford-Shah model, the constants c_1 and c_2 (which may be vectorial) are unknown and need to be solved for. In many applications, this might not be the case: The signature of objects of interest may be known in advance; in that case, the segmentation is a bit more elementary, since optimization over these parameters is no longer necessary. Nevertheless, it may very well be useful in other contexts to have the capability to solve for these constants if it becomes necessary. In that case, the optimal choice of the constants (i.e. their optimality condition) is well known:

$$
c_1 = \frac{\int_\Sigma f dxdy}{|\Sigma|} \quad \text{and} \quad c_2 = \frac{\int_{\Sigma^c} f dxdy}{|\Sigma^c|} \qquad (16)
$$

where the notation $|S|$ denotes the area of the set S. Implementing these formulas in our setting, where the boundary of the unknown set Σ is represented explicitly as a polygonal curve, requires some thought. Indeed, in order to evaluate the integrations over Σ involved in these formulas with subgrid accuracy, we need a little insight. The idea is to express the area integrals as path integrals, which is a standard exercise of Stokes' theorem in elementary vector calculus, like so:

$$\int_\Sigma f\, dxdy \;=\; \int_{\partial\Sigma} F\, n_x d\sigma \quad \text{where} \quad \frac{\partial F}{\partial x} = f. \tag{17}$$

Here, n_x denotes the x-component of the outer unit normal to the boundary $\partial\Sigma$ of the region Σ. The point is that there is, of course, a very natural way to approximate path integrals on polygonal curves numerically. Our algorithm for computing the integral $\int_\Sigma f\, dxdy$ is thus the following:

- Integrate f in the x-direction using the trapezoidal rule to define its primitive F on the grid so that $\frac{\partial f}{\partial x} = F$.
- Approximate the area integral as follows:

$$\int_\Sigma f\, dxdy \;=\; \int_{\partial\Sigma} F\, n_x d\sigma \;\approx\; \sum_{j=1}^{N} \frac{1}{2}\left[F(x_j, y_j) + F(x_{j+1}, y_{j+1})\right] \frac{D^+ y_j}{\sqrt{(D^+x_j)^2 + (D^+y_j)^2}}. \tag{18}$$

Note that the scheme involves interpolating F since (x_j, y_j) will of course not lie on grid points in general. With proper interpolation of F, the method is in fact *second order accurate*. Note also that the primitive (i.e. F) calculation needs to be done only once and is not repeated during the iterations of the gradient descent. Finally, note that $|\Sigma|$ can also be found with subgrid accuracy simply by using the above formula with $f \equiv 1$.

3.4 Variation of the Shape Prior and Scale Parameter Optimization

Variation of the shape prior (3) with respect to the vertex locations $\vec{p}_j$ of the evolving polygon is given by:

$$\frac{\partial}{\partial \vec{p}_k}\left(\alpha \sum_{i,j=1}^{N} \left(|\vec{p}_i - \vec{p}_j|^2 \;-\; s\, d_{i,j}^2\right)^2\right) \;=\; 8\alpha \sum_{j=1}^{N} \left(|\vec{p}_k - \vec{p}_j|^2 \;-\; s\, d_{kj}^2\right)(\vec{p}_k - \vec{p}_j)\cdot \vec{p}_k.$$

Hence, in gradient descent, the shape prior term contributes the velocity

$$\vec{v}_k^{\,shape} \;=\; \dot{\vec{p}}_k \;=\; -\alpha \sum_{j=1}^{N} \left(|\vec{p}_k - \vec{p}_j|^2 \;-\; s d_{kj}^2\right)(\vec{p}_k - \vec{p}_j). \tag{19}$$

Now, optimization with respect to the scale parameter s yields the following simple condition:

$$s \;=\; \frac{\sum_{i,j} |\vec{p}_i - \vec{p}_j|^2 d_{ij}^2}{\sum_{i,j} d_{ij}^4}. \tag{20}$$

3.5 Final Proposed Algorithm

Finally, putting everything together, the final complete gradient descent curve evolution equation for the proposed model is the ODE system:

$$\dot{\vec{p}}_k \;=\; \left[\left(\vec{v}_k^{\,per} \;+\; \vec{v}_k^{\,fid} \;+\; \vec{v}_k^{\,shape}\right)\cdot \vec{n}_k\right]\vec{n}_k \tag{21}$$

where $\vec{n}_k$ is the unit normal vector at the k-th vertex as defined in (14) and the velocities as obtained by calculating the variations in the perimeter, fidelity, and shape terms in the proposed model as seen above in (15) and (19) respectively. An explicit time marching scheme can be used for the gradient descent curve evolution equation above (21):

$$\vec{p}_k^{\,n+1} \;=\; \vec{p}_k^{\,n} \;+\; dt\left[\left(\vec{v}_k^{\,per} \;+\; \vec{v}_k^{\,fid} \;+\; \vec{v}_k^{\,shape}\right)\cdot \vec{n}_k\right]\vec{n}_k \tag{22}$$

Algorithm:

Step 1. Calculate the shape signature for the given reference shape via the symmetric matrix (3).
Step 2. Initialize the polygonal curve $\{\vec{p}_k\}_{k=1}^N$.
Step 3. Update the constants c_1 and c_2 via the formulas found in (16) where the area integrals are approximated by the scheme (18).
Step 4. Calculate the scale match via equation (20).
Step 5. Finally, evolve the polygonal curve via the iteration scheme in (22).

Repeat **Steps 3** through **5** as needed until the curve reaches a fixed contour.

We remark that the starting point of the parametrization of the shape prior can have an effect on the minimization of the shape signature term (3). In particular, suppose a given shape has two different parametrizations: $\Sigma_1 = \{\vec{p}_j\}_{j=1}^N$ and $\Sigma_2 = \{\vec{q}_j\}_{j=1}^N$, both differing only in a shift of the starting point of one of the parametrizations. Let σ be a forward shift operator on the indices j by some set amount K. Thus, Σ_1 and Σ_2 represent the same shape, but Σ_2 is obtained by Σ_1 via the operation $\vec{p}_j = \vec{q}_{\sigma(j)} = \vec{q}_{j+K}$ under periodic boundary conditions on the indices. Then, the cliques energy (3) comparing these two shapes will not be minimized due to the parametrization mismatch, even though the shapes are exactly the same.

One simple way to bypass this particular caveat when minimizing the proposed energy is to initially start with a fixed small shape parameter and then repeatedly minimizing the proposed energy over the set of forward shifts of the shape prior parametrization. Here, we shift the starting point of the indices by some fixed amount, either 2 ,3, or 4 etc. depending on how many points on the evolving polygon are used. This allows a set of solution curves ϕ_k that can then be placed into the proposed energy (4). Then, the parametrization shift corresponding to the minimum of the set $\{E_{MSWS}(\phi_k)\}_{k=1}^M$ is then applied to the shape prior S, and this new prior $\overline{S}$ is then used as the effective prior for the segmentation.

We also mention that two different initial conditions can be used for minimizing the proposed model, namely:

1. starting with the initial contour obtained from the standard (no-shape) MS model (1) and then gradually turning up the shape parameter α during the minimization of the proposed one.
2. starting from the initial contour (circle, ellipse, etc.) and using a small initial shape parameter, then gradually turning it up.

The decision is based on how well the initial MS (no-shape) segmentation approximates the object of interest. To avoid this dependence, we advocate utilizing approach 2 since from the very start of the minimization process, the shape term directly has an effect on the segmentation. Nonetheless, we have found that similar results are obtained in either case, and in the next section, we will show numerical experiments detailing both approaches.

4 Numerical Experiments

4.1 Airplane Segmentation Example

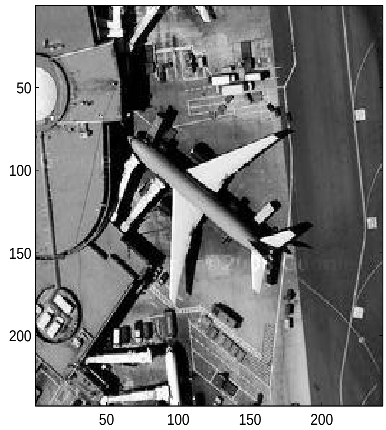

(a) Reference Image

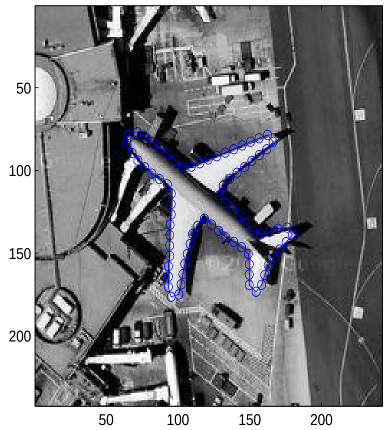

(b) Reference Image
w/ Learned Reference Shape

Figure 2: *Segmentation with Learned Reference Shape*

One of the most difficult objects to segment are those that have portions within the object with image intensities close to that of the background. In addition, clutter or other surrounding objects further compound the task as well. One particular object that has seen quite a bit of interest recently in regards to segmentation is that of an airplane, which is often viewed from satellite surveillance data. Aircraft in general, prove difficult to segment due to the issues with the fuselage, wings, or other structure having little contrast variation from the tarmac or surrounding airport structures.

In Fig. 2 (a) a reference image of a real airplane obtained from satellite data is observed and it's subsequent segmentation (learned shape) by hand can be seen in Fig. 2 (b). In Fig. 3 (a), an image of a different plane (to be segmented) is observed. The standard (no shape) segmentation of this particular plane will prove difficult since many components match the background and underlying airport structure. For example, the wings, engines, and rear winglets have intensities similar to parts of the building (white) and loading infrastructure. In addition, the fuselage of the plane is nearly the same intensity as the surrounding tarmac and adjacent building. The learned shape prior juxtaposed against the plane to be segmented is viewed in Fig. 3 (b).

In Fig. 4 (a) an initial circle contour is observed. We then set the initial shape parameter to be equal to 0.1 and run the proposed method to obtain the segmentation result in 4 (b) where already, the contour is approaching that of the plane. In 4 (c)–(d), we increase the shape parameter through the values 0.3 and 0.5 respectively and the plane becomes nearly segmented. Finally, in Fig. 5 (a)–(c), the shape parameter is increased through larger values of 0.7, 0.9, and lastly to 1.0 respectively. Remarkably, a cleanly segmented plane is obtained despite the complexities in the segmentation. In Fig. 5 (d), the result via the standard piece-wise constant Mumford Shah model (1) without a shape term is observed where the model segments a large region nowhere near the boundary of the airplane. This should be expected due to the difficulties with this particular segmentation.

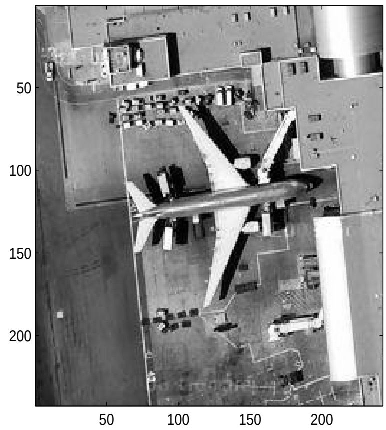

(a) Image to be Segmented

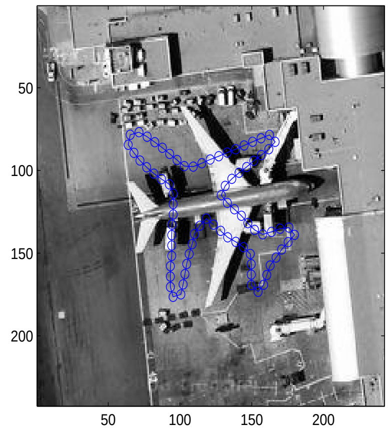

(b) Image to be Segmented
w/ Learned Reference Shape

Figure 3: *Segmentation with Learned Reference Shape*

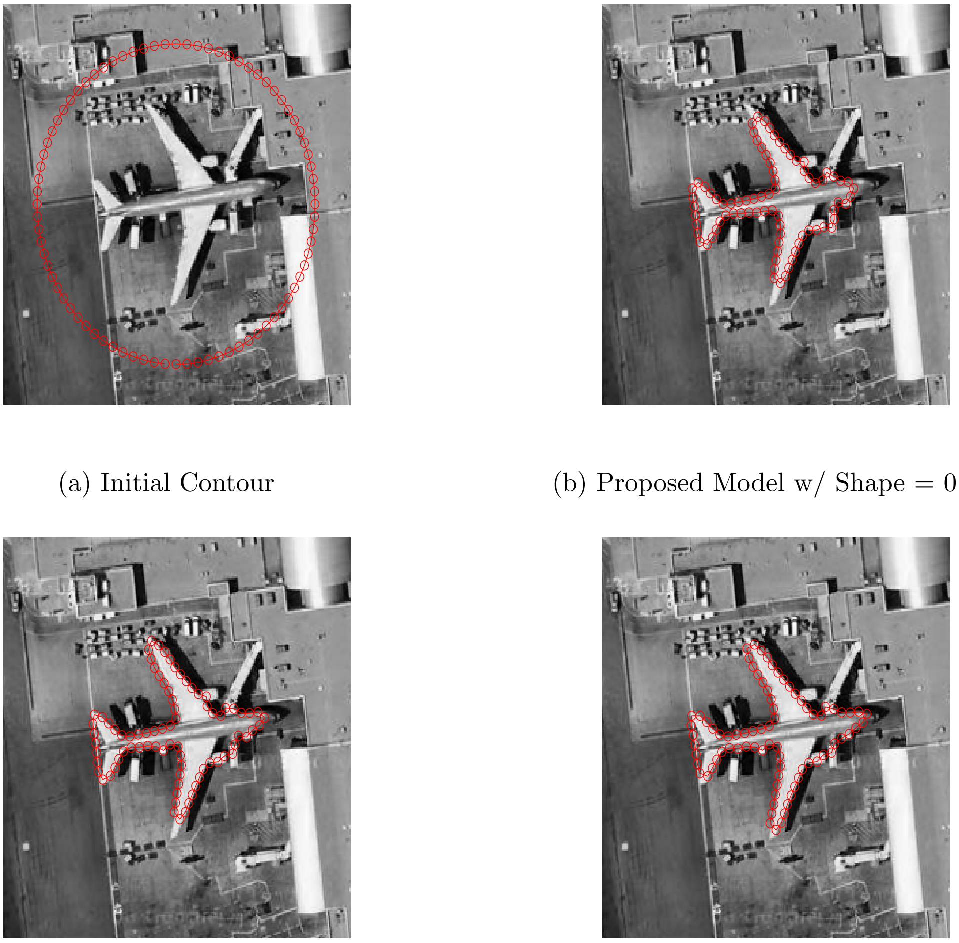

(a) Initial Contour

(b) Proposed Model w/ Shape = 0.1

(c) Proposed Model w/ Shape = 0.3

(d) Proposed Model w/ Shape = 0.5

Figure 4: *Segmentation Results with Learned Reference Shape*

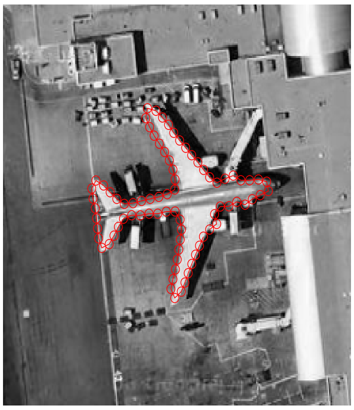

(c) Proposed Model w/ Shape = 0.7

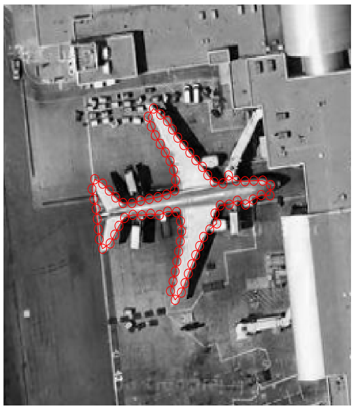

(d) Proposed Model w/ Shape = 0.9

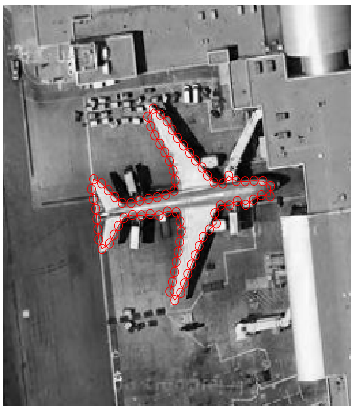

Proposed Model w/ Shape = 1.0

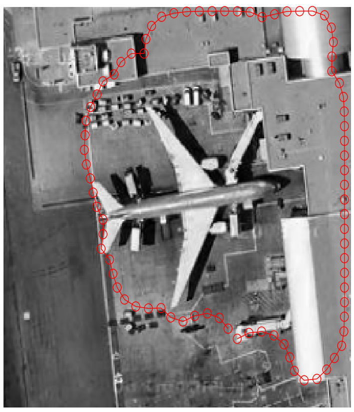

Standard PPWCMS
(No Shape)

Figure 5: *Segmentation Results with Learned Reference Shape*

4.2 Disocclusion Experiments

4.2.1 Book Disocclusion Example

In this example we demonstrate how the proposed model can be used for image disocclusion. If we let $R \subseteq \mathbb{R}^2$ denote the region to be disoccluded, we simply make the small change in the proposed model (4) by replacing λ by $\lambda(1-\chi_R)$ with χ_R defined by:

$$\chi_R = \begin{cases} 1 & \text{if } \vec{x} \in R \\ 0 & \text{otherwise.} \end{cases} \tag{23}$$

A clean book image is observed in Fig. 6 (a), while in Fig. 6 (b), the same book at a different scale with an occlusion can be seen. Here, the corner of the white book is occluded by the black one. In Fig. 6 (c), the indicator for the occluder region: $1-\chi_R$ is observed. Since it is available, we use the clean un-occluded book seen in Fig. 6 (a) as the shape prior and this contour is viewed in Fig. 6 (d). The initial contour for the disocclusion problem and the image to be disoccluded is observed in Fig. 7 (a) and the result from the standard polygonal piecewise constant Mumford-Shah functional is seen in 7 (b). As expected, the corner of the book is not disoccluded and only the observable region is segmented. We then use this contour from the standard Mumford-Shah segmentation as an initial contour for our shape prior model, where, in Fig. 8 (a), upon setting the initial shape parameter to 0.1, and running the proposed method, the image begins to become disoccluded. As the shape term is increased further to 0.5 and 0.9 as observed in Fig. 8 (b) and (c) respectively, the image becomes successfully disoccluded and the complete boundary of the book is found. We remark that the scale parameter is automatically found during the curve evolution using the minimization condition in equation (20).

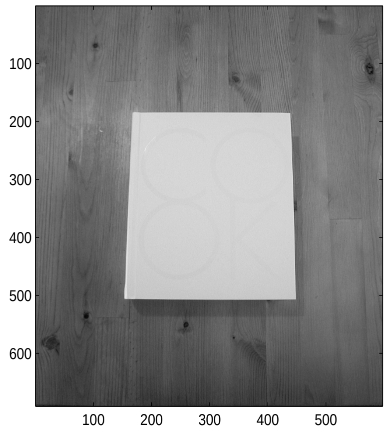

(a) Book Image

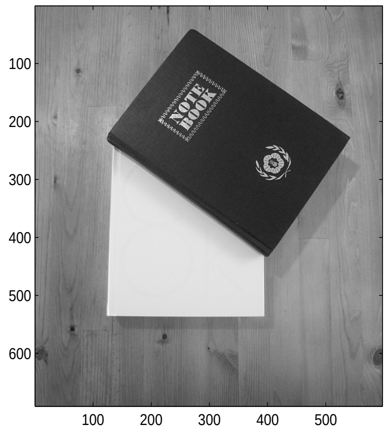

(b) Occluded Book Image

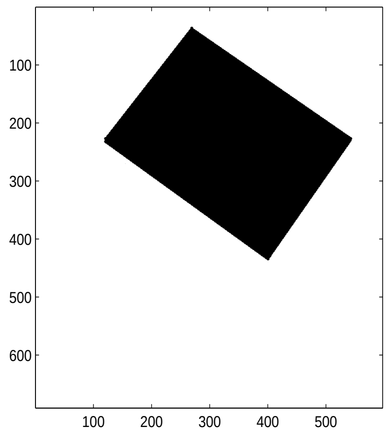

(c) Indicator Function of Occluder
(Found via Segmentation)

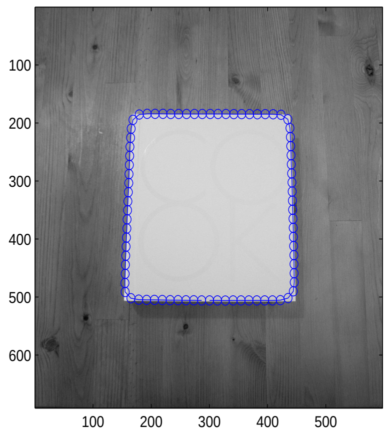

(d) Reference Shape Contour
(Different Scale than Occluded Book)

Figure 6: *Book Disocclusion*

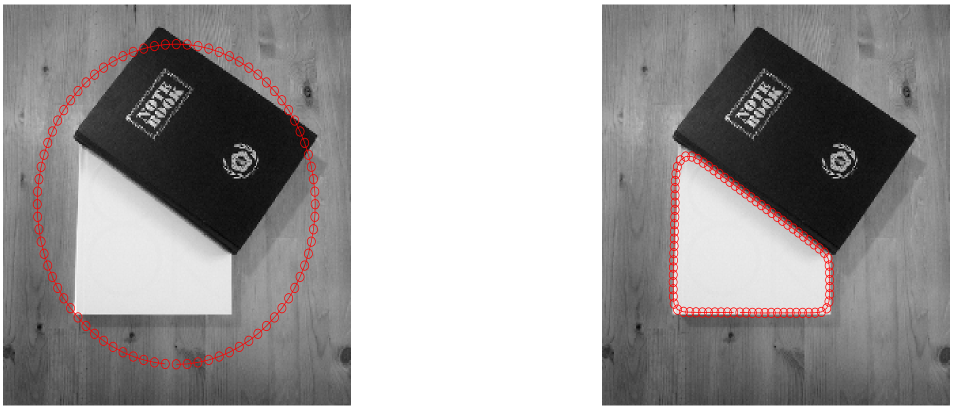

(a) Initial Contour

(b) Segmented Image via PPCMS (No Shape)

Figure 7: *Book Disocclusion Results: Automatic Scale Search*

(a) Segmented Image w/ Shape Prior
(Shape parameter set to 0.1)

(b) Segmented Image w/ Shape Prior
(Shape parameter set to 0.5)

(c) (Shape parameter set to 0.9)

Figure 8: *Book Disocclusion Results: Automatic Scale Search* As the shape parameter approaches 1, the image becomes completely disoccluded. Scale and the constants c_1 and c_2 are found automatically.

4.2.2 Averaging Priors: Book Disocclusion Example Revisited

In this next experiment, we use the averages of a particular set of shapes as a shape prior. This process is often utilized in machine learning where a library of given shapes is available. Either by first preprocessing the shapes via registration if the signature is not invariant to rigid motion, or in our case, without any alignment needs, one can compute the average shape with respect to a given shape signature. A recent work concerning the averaging of shape priors can be found at [34]; further references regarding shape averaging can also be found therein. For our purposes, the average of the priors is taken with respect to the cliques signature. Then the computed (average) shape prior is then utilized in image segmentation. We outline this procedure below:

Let $\Omega_1, \Omega_2, \ldots, \Omega_M$ be given polygons representing shapes. Here, each polygonal curve Ω_m has vertices $\vec{q}_1^{\,m}, \vec{q}_2^{\,m}, \ldots, \vec{q}_N^{\,m}$ indexed in counterclockwise order. Let Γ denote the average polygon with respect to the proposed 'cliques' invariant signature (3). Here, $\{\vec{p}_1, \ldots, \vec{p}_N\}$ are the unknown vertices of Γ which are to be solved for. We also let $d(\Gamma) = (d_{i,j})_{i,j=1}^{N}$ the symmetric matrix of intervertex distances of the average shape. Additionally, let $d_S(\Gamma)$ denote the shifts to the right of the columns of $d(\Gamma)$ under periodic boundary conditions. e.g. $d_N(\Omega) = d_0(\Omega) = d(\Omega)$. Then, to calculate the average shape with respect to the 'cliques' signature, we consider the following minimization problem:

$$\min_{\Gamma} \sum_{m=1}^{M} \min_{S} ||d_S(\Gamma) - d(\Omega_m)||_2^2.$$

Discretely, assuming the inner minimization with respect to the shifts S is obtained (e.g. the correct location to start the parametrization is obtained), then the problem reduces to:

$$\min_{p_1, p_2, \ldots, p_N} \sum_{m=1}^{M} \left(\sum_{i,j=1}^{N} \left(|\vec{p}_i - \vec{p}_j|^2 - |\vec{q}_i^{\,m} - \vec{q}_j^{\,m}|^2 \right)^2 \right). \tag{24}$$

The minimization of the above quantity (24) contributes the velocity to the evolution of the polygon:

$$\vec{v}_k = -\sum_{m=1}^{M} \sum_{j=1}^{N} \left(|\vec{p}_k - \vec{p}_j|^2 - |\vec{q}_k^{\,m} - \vec{q}_j^{\,m}|^2 \right) (\vec{p}_k - \vec{p}_j).$$

Thus, if $\vec{N}_k$ is the unit normal vector to the polygonal curve at the vertex $\vec{p}_k$, then the ODE equation for gradient descent for evolving the polygonal curve in the normal direction is given by:

$$\dot{\vec{p}_k} = \left(\vec{N}_k \cdot \vec{v}_k \right) \vec{N}_k. \tag{25}$$

The steady state solution to the above equation (25) will yield the averaged shape with respect to the 'cliques' signature (3).

In the following example, we use $M = 4$ in the above procedure (24), thus averaging 4 shapes into a single prior. In Fig. 9, four perturbations of a square shape are observed. In Fig. 10 (a), the clean unperturbed shape is observed while in 10 (b), the the result from the evolution equation (25) for averaging the priors from Fig. 10 (a) is observed as the blue contour where the averaged prior still has the initial underlying square shape. In Fig. 10 (c), an occluded image with the averaged shape prior (shown is blue) is observed, the scale differential should be noted between the prior and the image to be disoccluded. In Fig. 11 (a) the, initial contour obtained from the standard PPCMS model is observed. The final result obtained from the proposed model using the averaged shape prior is observed in 10 (b). This result was found by increasing the shape parameter through values 0.1, 0.5, 0.9, and finally to 1.0 respectively. Once again, the scale parameter 's' is automatically found via equation (20) during the minimization of the proposed model. As observed in Fig. 11 (b), the book is successfully disoccluded using the average of the four shape priors observed in Fig. 10.

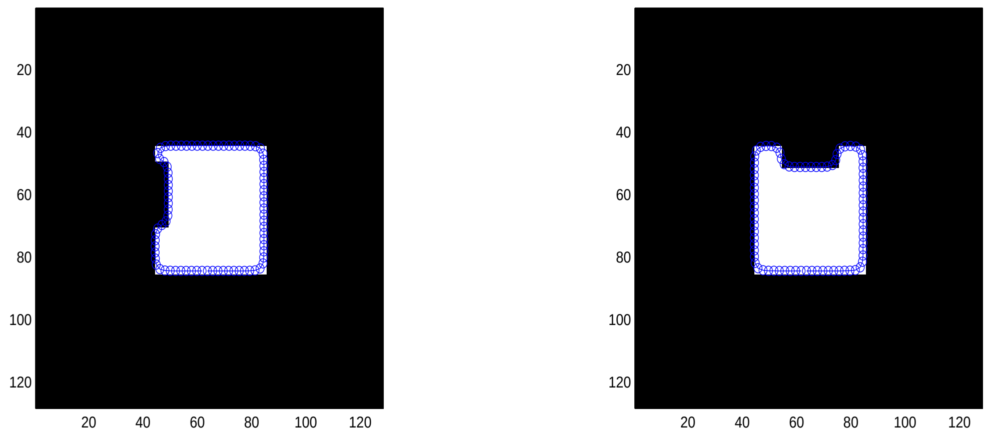

Perturbations of Square w/ Segmentation shown in blue

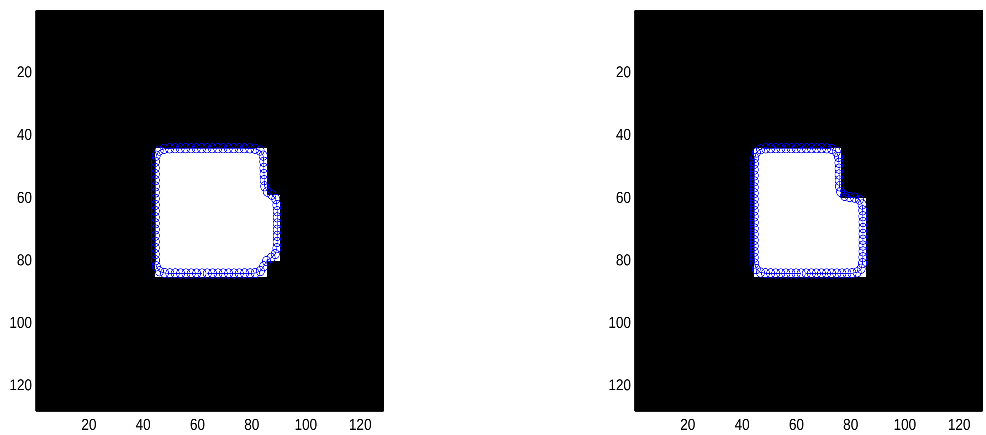

Perturbations of Square w/ Segmentation shown in blue

Figure 9: *Averaging Priors:* Perturbations of the Shape Prior

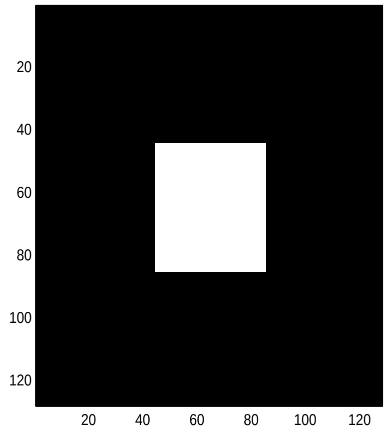

(a) Unperturbed Shape Prior Image (Square)

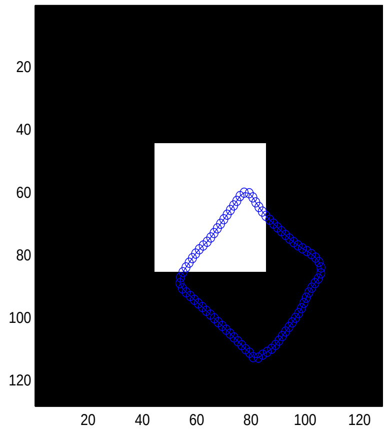

(b) Result of Averaging Priors (blue)

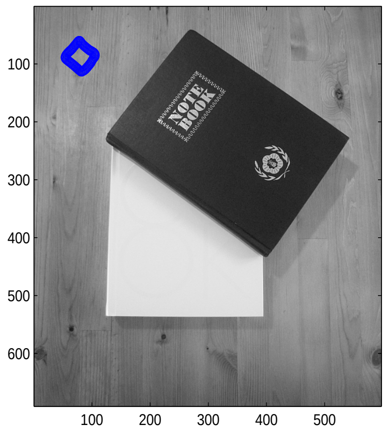

Occluded Image (white book) and Avg'd. Shape Prior of Different Scale (blue)

Figure 10: *Averaging Priors*

(a) Initial Contour (From PPCMS) (b) Result w/ Shape = 1.0

Figure 11: *Disocclusion with Averaged Priors:* Optimization Method Starting w/ initial contour from segmentation of the standard Mumford Shah Model. Shape prior is scaled automatically during the optimization. All constants c_1 and c_2 are updated throughout and the final result is obtained by increasing the shape parameter through values 0.1, 0.3, $\ldots$, 0.9, 1.0. The final result is viewed in (b) where, despite using the averaged shape priors, the book is successfully disoccluded.

4.2.3 Maple Leaf Disocclusion

In this example, we choose to disocclude an object with some more subtle geometric features on its boundary, in this case a maple leaf. In Fig. 12 (a), a clean maple leaf is observed while in 12 (b), the occluded image can be seen. We choose to use another maple leaf as a reference image having a scale roughly 40% that of the image to be disoccluded. This image can be seen in 12 (c), while the shape prior obtained from segmenting the reference image is observed in Fig. 12 (d) as the blue contour. To better show the scale differential, the clean image and learned shape (blue) are shown in Fig. 13 (a). The image to be disoccluded and initial contour for the proposed segmentation process are both observed in Fig. 13 (b). The final disocclusion results from the proposed model are shown in Fig. 13 (c). This result was obtained by increasing the shape parameter from an initial value of 0.1 through values 0.3, 0.5, 0.7, and 0.9 respectively. The final result with the disocclusion mask removed can be seen in Fig. 13 (d) showing a successful disocclusion. The shape parameter was chosen from searching through a manual range of scales. In this particular experiment, the value for the parameter 's' is 0.43.

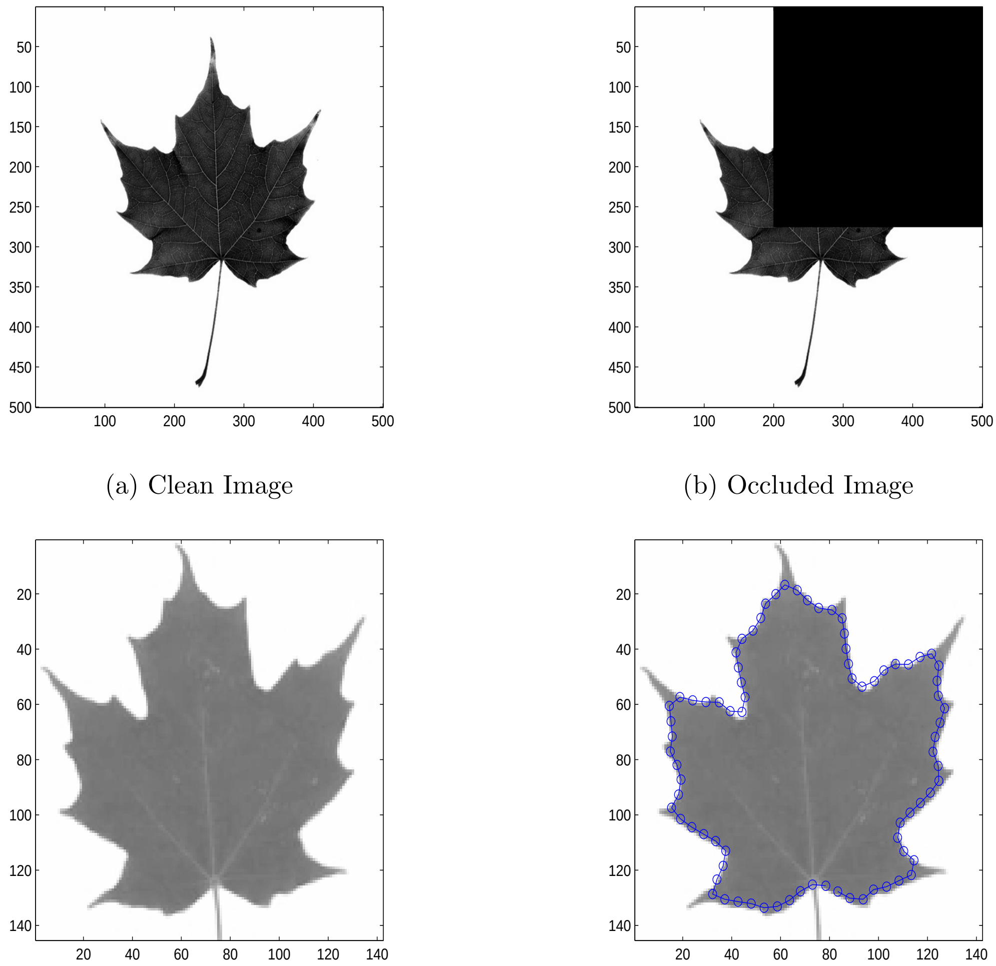

(a) Clean Image

(b) Occluded Image

(c) Reference Image

(d) Reference Image and Learned Shape

Figure 12: *Dissocclusion of a Maple Leaf*

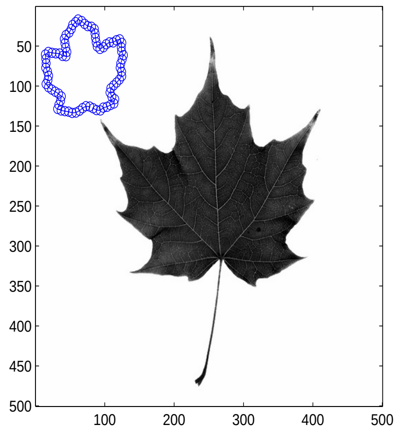

(a) Clean Image and Learned Shape (Note Scale Differential)

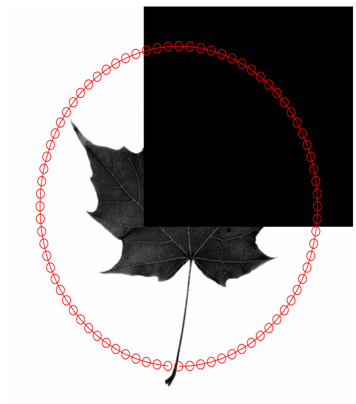

(b) Initial Contour

(c) Disocclusion

(d) Disocclusion with Mask Removed

Figure 13: *Disocclusion of a Maple Leaf* Manual range of scales search. Fidelity Param. set to 16 and Shape increased from 0.1, 02, . . . , 0.9, 1.0.

4.3 Difficult Segmentation: Explicit Example

In this culminating example, we segment what is considered to be a difficult case. In Fig. 14 (a), a reference image and shape prior (in blue) is observed while in (b), a clean image (to be segmented) is seen. The image in (b) is of particular interest since the color of the fuselage matching that of the surrounding tarmac makes this case very difficult due to the ambiguities of the region to be segmented. Further compounding this particular case is the observation that the flight equipment around the plane (clutter) also has similar contrast to the planes wings. In addition, the white fuselage and wings of the adjacent plane also has the same contrast as the wings of the plane to be segmented.

In Fig. 15 (a), the initial contour for our segmentation procedure is observed. The proposed model is then minimized by gradually increasing the shape strength constant (in increments of 0.2) through values from 0.1 to 1.0. The results from the proposed model with shape strength equaling 0.1, 0.5, and finally 1.0 are observed in Fig. 15 (b)–(d). Right from the start, even though the shape strength term has value only 0.1, the plane has already become segmented. The final segmentation result is observed in 15 (d) where the shape term has value 1.0 and the correct plane is accurately segmented despite the clutter around the plane and the fuselage having nearly the same contrast as the surrounding tarmac. The result from the standard (no shape) Mumford-Shah model is observed in Fig. 15 (e), where the plane is nowhere near correctly segmented. Lastly, we remark that the scale parameter 's' in this experiment was manually chosen over a range of scales.

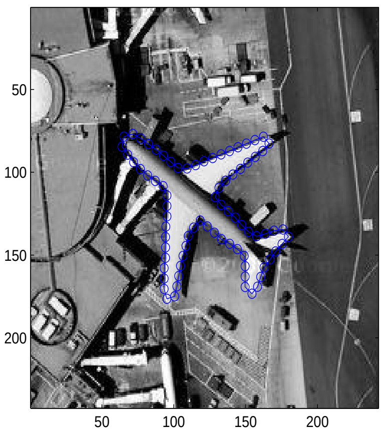

(a) Reference Image
with Learned Reference Shape (blue)

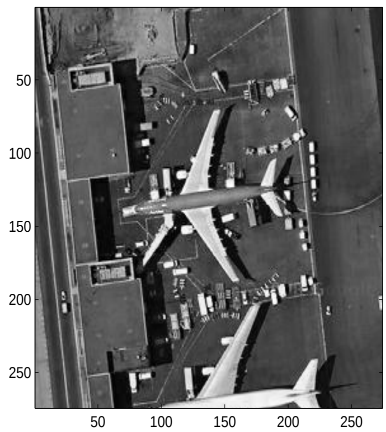

(b) Image to be Segmented

Figure 14: *Learned Reference Shape*

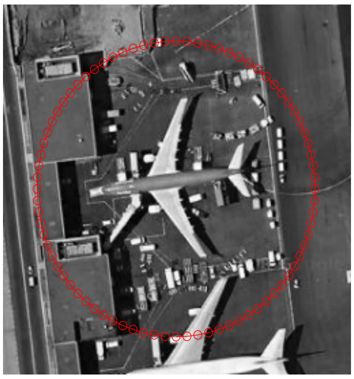

(a) Initial Contour

(b) Proposed w/ Shape Param. set to 0.1

(c) Proposed w/ Shape Param. set to 0.5

(d) Proposed w/ Shape Param. set to 1.0

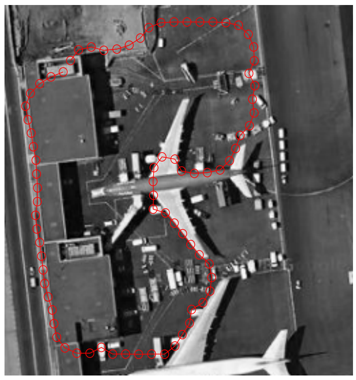

(e) Result with no Shape (Standard Mumford Shah)

Figure 15: *Segmentation results with Learned Reference Shape*

5 Conclusions and Future Work

We proposed an efficient and nearly automated shape prior segmentation model and executed many compelling numerical tests that successfully showed the usefulness of the algorithm for segmentation amidst clutter and also segmenting particular objects having regions of non-uniform contrasts. Additionally, we showed how the model can be used for applications in image disoclussion. Some future work includes the following:

1. **Better Initial Contour**
   We utilized two different ways to run the segmentation procedure:
   - Begin with an arbitrary circle/ellipse as the initial contour while using a small initial shape term. Then running the algorithm while gradually increasing the shape parameter.
   - Run the standard PPCMS (no shape) segmentation and use this result as the initial contour for the proposed model. Here, we then run the proposed method by gradually increasing the shape term until a final contour is reached.

   Unfortunately, starting with an arbitrary contour (circle/ellipse) far away from the object to be segmented may result in local minima (e.g. improperly segmented regions). On the other hand, oftentimes the standard PPCMS (no shape) model may segment some objects far from the one in interest. Thus, using this as a starting point may yield incorrect segmentations. Perhaps generating a coarse initial contour using some feedback from the shape signature would be a good place to start.
2. **Finer Segmentations**
   Possibility to use local gradient information to achieve closer and or finer segmentations based on the methodologies in the TVG/CVG/Active-Contour models seen in [8].
3. **Release Quality Code** At this point, we are working on release quality code utilizing a GUI interface which will be found on the authors website: 'www.math.uci.edu/~fepark'.

6 Acknowledgements

The author learned about the use of "cliques" for shape comparison – which is incorporated into Mumford-Shah based image segmentation in this paper – from Prof. Ron Kimmel by way of Selim Esedoglu; he thanks them both. Lastly, the author would like to once again thank Selim Esedoglu and also Hongkai Zhao for their encouragement with this project.

References

[1] L. Ambrosio, N. Fusco, and P. Pallara, *Functions of Bounded Variation and Free Discontinuity Problems.* Oxford University Press, 2000.

[2] L. Ambrosio and V. M. Tortorelli, Approximation of functionals depending on jumps by elliptic functionals via Γ-convergence. *Communications on Pure and Applied Mathematics*, XLIII:999-1036, 1990.

[3] X. Bresson and T. F. Chan, Non-local Unsupervised Variational Image Segmentation Models. UCLA CAM Report 08-67, 2008.

[4] X. Bresson, S. Esedoglu, P. Vandergheynst, J. Thiran, and S. Osher. Fast Global Minimization of the Active Contour/Snake Models. *Journal of Mathetimatical Imaging and Vision*, 28(2):151-167, 2007.

[5] X. Bresson, P. Vandergheynst, and J. Thiran A Variational Model for Object Segmentation Using Boundary Information and Shape Prior Driven by the Mumford-Shah Functional, *International Journal of Computer Vision (IJCV)*, 28(2):145 - 162, 2006.

[6] A. Bronstein, M. Bronstein, and R. Kimmel, *Numerical Geometry of Non-Rigid Shapes*, Monographs in Computer Science. Springer, 2008.

[7] D. Cremers and N. Sochen *Towards Recognition-Based Variational Segmentation Using Shape Priors and Dynamic Labeling*, *Lecture Notes in Computer Science*. 2695:388-400, 2003.

[8] X. Bresson, S. Esedoglu, P. Vandergheynst, J. Thiran, S. Osher, Fast Global Minimization of the Active Contour/Snake Model, Journal of Mathematical Imaging and Vision, v.28, pp.151-167, 2007.

[9] A. M. Bronstein, M. M. Bronstein, and R. Kimmel. Three-dimensional face recognition, *International Journal of Computer Vision*. 64(1):5-30, 2005.

[10] A. M. Bronstein, M. M. Bronstein, and R. Kimmel, Expression-invariant representations of faces, *IEEE Trans. Image Processing*, 16(1):188-197, 2007.

[11] V. Caselles, R. Kimmel, and G. Sapiro. Geodesic Active Contours. *International Journal of Computer Vision*, 22(1):61-79, 1997.

[12] A. Chambolle. An Algorithm for Total Variation Minimization and Applications. *Journal of Mathematical Imaging and Vision*, 20(1-2):89-97, 2004.

[13] T. F. Chan, S. Esedoglu, and M. Nikolova. Algorithms for Finding Global Minimizers of Image Segmentation and Denoising Models. *SIAM Journal on Applied Mathematics*, 66(5):1632-1648, 2006.

[14] Y. Chen, H. Tagare, S. Thiruvenkadam, F. Huang, D. Wilson, K. Gopinath, R. Briggsand, and E. Geiser. Prior Shapes in Geometric Active Contours in a Variational Framework. *International Journal of Computer Vision*, 50(3):315-328, 2002.

[15] T. F. Chan and L. A. Vese. Active Contours Without Edges. *IEEE Transactions on Image Processing*, 10(2):266-277, 2001.

[16] Y. Chen, H. D. Tagare, S. Thiruvenkadam, F. Huang, D. Wilson, K. S. Gopinath, R. W. Briggsand, and E. A. Geiser. Using Prior Shapes in Geometric Active Contours in a Variational Framework. *International Journal of Computer Vision*, 50(3):315-328, 2002.

[17] I. Ekeland and R. Temam. *Convex Analysis and Variational Problems*. North Holland, Amsterdam, 1976.

[18] A. Elad and R. Kimmel. On Bending Invariant Signatures for Surfaces. *IEEE Transactions on Pattern Analysis and Machine Intelligence*, 25(10):1285-1295, 2003.

[19] G. Gilboa and S. Osher. Nonlocal Linear Image Regularization and Supervised Segmentation. *SIAM Multiscale Modeling and Simulation (MMS)*, 6(2):595-630, 2007.

[20] T. Goldstein and S. Osher. The Split Bregman Method for L1 Regularized Problems, *SIAM Journal on Imaging Sciences*. 2(2):323-343, 2009.

[21] N. Houhou, J.-P. Thiran, and X. Bresson. Fast Texture Segmentation Model based on the Shape Operator and Active Contour. In *IEEE Conference on Computer Vision and Pattern Recognition*, 2008.

[22] M. Kass, A. Witkin, and D. Terzopoulos. Snakes: Active Contour Models. *International Journal of Computer Vision*, pages 321-331, 1987.

[23] K. Kolev, M. Klodt, T. Brox, S. Esedoglu, and D. Cremers. Continuous Global Optimization in Multiview 3D Reconstruction. In *Energy Minimization Methods in Computer Vision and Pattern Recognition (EMMCVPR)*, volume 4679, pages 441-452, 2007.

[24] G. Kuhne, J. Weickert, M. Beier, and W. Effelsberg. Fast Implicit Active Contour Models. In *DAGM Symposium on Pattern Recognition*, pages 133-140, 2002.

[25] S. Leung and S. Osher. Global Minimization of the Active Contour Model with TV-Inpainting and Two-Phase Denoising. In *Variational, Geometric, and Level Set Methods in Computer Vision (VLSM), Springer-Verlag*, vol. 3752, pages 149-160, 2005.

[26] M. Leventon, W. Grimson, and O. Faugeras. Statistical Shape Influence in Geodesic Active Contours. In *International Conference of Computer Vision and Pattern Recognition*, pages 316-323, 2000.

[27] C. Li, C.-Y. Kao, J. C. Gore, and Z. Ding. Implicit Active Contours Driven by Local Binary Fitting Energy. In *Computer Vision and Pattern Recognition (CVPR)*, pages 1-7, 2007.

[28] C. Li, C.-Y. Kao, J. C. Gore, and Z. Ding. Minimization of Region-Scalable Fitting Energy for Image Segmentation. *IEEE Transactions on Image Processing*, 17(10):1940-1949, 2008.

[29] J.-M. Morel and S. Solimini, *Variational models in image segmentation.* Birkäuser, 1994.

[30] J.-M. Morel and S. Solimini, *Segmentation of images by variational methods: a constructive approach*, Revista Matematica de la Universidad Complutense de Madrid, 1(1):169-182, 1988.

[31] B. Mory and R. Ardon. Fuzzy Region Competition: A Convex Two-Phase Segmentation Framework. In *Scale Space Variational Methods (SSVM)*, pages 214-226, 2007.

[32] D. Mumford and J. Shah. Optimal Approximations of Piecewise Smooth Functions and Associated Variational Problems. *Communications on Pure and Applied Mathematics*, 42:577-685, 1989.

[33] K. Ni, X. Bresson, T. Chan, and S. Esedoglu. Local Histogram-Based Segmentation Using the Wasserstein Distance. *International Journal of Computer Vision*, 84(1):97-111, 2009.

[34] M. Rumpf and B. Wirth. A Nonlinear Elastic Shape Averaging Approach. *SIAM Journal on Imaging Sciences*, 2(3):800-833, 2009.

[35] S. Osher. "Level Set Methods", in Geometric Level Set Methods in Imaging, Vision and Graphics. *eds. S. Osher and N. Paragios, Springer-Verlag, NY*, pages 3-20, 2003.

[36] S. Osher and N. Paragios. *Geometric Level Set Methods in Imaging, Vision and Graphics.* Springer-Verlag, NY, 2003.

[37] S. Osher and J. A. Sethian. Fronts Propagating with Curvature-Dependent Speed: Algorithms Based on Hamilton-Jacobi Formulations. *Journal of Computational Physics*, 79(1)(12-49), 1988.

[38] P. Perona and J. Malik. Scale-Space and Edge Detection Using Anisotropic Diffusion. *IEEE Transactions on Pattern Analysis and Machine Intelligence*, 1252(629-639), 1990.

[39] L. I. Rudin, S. Osher, and E. Fatemi. Nonlinear Total Variation Based Noise Removal Algorithms. *Physica D*, 60(1-4):259-268, 1992.

[40] [47] J. A. Sethian. *Level Set Methods and Fast Marching Methods: Evolving Interfaces in Computational Geometry, Fluid Mechanics, Computer Vision and Material Sciences*. Cambridge University Press, 1999.

[41] M. Unger, T. Pock, and H. Bischof. Continuous Globally Optimal Image Segmentation with Local Constraints. In *Computer Vision Workshop*, 2008.

[42] [50] L. A. Vese and T. F. Chan. A Multiphase Level Set Framework for Image Segmentation Using the Mumford and Shah Model. *International Journal of Computer Vision*, 50(3):271-293, 2002.

[43] A. Yezzi, L. Zöllei, and T. Kapur, A variational framework for integrating segmentation and registration through active contours, *Medical Image Analysis*, 7(2):171-185, 2003.

[44] H. Zhao, T. Chan, B. Merriman, and S. Osher. A Variational Level Set Approach to Multiphase Motion. *Journal of Computational Physics*, 127(167):179-195, 1996.

[45] H. Zhao, S. Osher, B. Merriman, and M. Kang. Implicit and Nonparametric Shape Reconstruction from Unorganized Data using a Variational Level Set Method. *Computer Vision and Image Understanding*, 80(3):295-314, 2001.

[46] T. F. Chan, W. Zhu. Level Set Based Shape Prior Segmentation. *In Proc. CVPR05*, pages:295-314, 2005.

[47] S. C. Zhu and A. Yuille. Region Competition: Unifying Snakes, Region Growing, and Bayes/MDL for Multiband Image Segmentation. *IEEE Transactions on Pattern Analysis and Machine Intelligence*, 18(9):884-900, 1996.